The crystal structure of vascular endothelial growth factor (VEGF) refined to 1.93 Å resolution: multiple copy flexibility and receptor binding

Yves A Muller[1†], Hans W Christinger[1], Bruce A Keyt[2] and Abraham M de Vos[1*]

Background: Vascular endothelial growth factor (VEGF) is an endothelial cell-specific angiogenic and vasculogenic mitogen. VEGF also plays a role in pathogenic vascularization which is associated with a number of clinical disorders, including cancer and rheumatoid arthritis. The development of VEGF antagonists, which prevent the interaction of VEGF with its receptor, may be important for the treatment of such disorders. VEGF is a homodimeric member of the cystine knot growth factor superfamily, showing greatest similarity to platelet-derived growth factor (PDGF). VEGF binds to two different tyrosine kinase receptors, kinase domain receptor (KDR) and Fms-like tyrosine kinase 1 (Flt-1), and a number of VEGF homologs are known with distinct patterns of specificity for these same receptors. The structure of VEGF will help define the location of the receptor-binding site, and shed light on the differences in specificity and cross-reactivity among the VEGF homologs.

Results: We have determined the crystal structure of the receptor-binding domain of VEGF at 1.93 Å resolution in a triclinic space group containing eight monomers in the asymmetric unit. Superposition of the eight copies of VEGF shows that the β-sheet core regions of the monomers are very similar, with slightly greater differences in most loop regions. For one loop, the different copies represent different snapshots of a concerted motion. Mutagenesis mapping shows that this loop is part of the receptor-binding site of VEGF.

Conclusions: A comparison of the eight independent copies of VEGF in the asymmetric unit indicates the conformational space sampled by the protein in solution; the root mean square differences observed are similar to those seen in ensembles of the highest precision NMR structures. Mapping the receptor-binding determinants on a multiple sequence alignment of VEGF homologs, suggests the differences in specificity towards KDR and Flt-1 may derive from both sequence variation and changes in the flexibility of binding loops. The structure can also be used to predict possible receptor-binding determinants for related cystine knot growth factors, such as PDGF.

Addresses: [1]Department of Protein Engineering, Genentech, Inc., 460 Point San Bruno Boulevard, South San Francisco, CA 94080, USA and [2]Department of Cardiovascular Research, Genentech, Inc., 460 Point San Bruno Boulevard, South San Francisco, CA 94080, USA.

[†]Present address: Forschungsgruppe Kristallographie, Max-Delbrück-Centrum für Molekulare Medizin, Robert-Rössle-Straße 10, D-13122 Berlin-Buch, Germany.

*Corresponding author.
E-mail: devos@gene.com

Key words: angiogenesis, cystine knot, multiple conformations, receptor specificity, vascular permeability factor

Received: **25 July 1997**
Revisions requested: **26 August 1997**
Revisions received: **29 August 1997**
Accepted: **29 August 1997**

Structure 15 October 1997, **5**:1325–1338
http://biomednet.com/elecref/0969212600501325

Introduction

Angiogenesis is the sprouting of blood capillaries from pre-existing blood vessels, while vasculogenesis is the *de novo* development of blood vessels through differentiation of early endothelial cells during embryonic development [1]. Vascular endothelial growth factor (VEGF) has been identified as an endothelial cell-specific mitogen mediating both of these processes [1–4]. Heterozygous knock-out mice lacking a single VEGF allele are not viable beyond days 11 and 12 in the uterus and show severe abnormal blood vessel formation [5,6].

Angiogenesis plays a critical role in the pathogenesis of a variety of disorders such as cancer, proliferative retinopathy and rheumatoid arthritis [1]. Tumor vascularization is required to overcome tumor ischemia and necrosis; furthermore, aggressive behavior of different carcinomas correlates strongly with the degree of tumor vascularization [2]. VEGF is released by a variety of tumors; tumor growth can be suppressed by the administration of anti-VEGF antibodies *in vivo* [7]. In addition, diabetic retinopathy, a leading cause of blindness caused by excessive intraocular neovascularization, has been linked to elevated VEGF levels in the eye [8,9]. At the atomic level, these physiological events are initiated by the specific interaction of VEGF with two receptors, kinase domain receptor (KDR) and Fms-like tyrosine kinase 1 (Flt-1). Therefore, VEGF antagonists preventing this interaction might play an important role in the effective treatment of tumors as well as pathogenic vascularization in general.

VEGF is a glycosylated, disulfide-linked homodimer and is expressed in different isoforms ranging in size from 121 to 206 residues in humans ($VEGF_{121}$, $VEGF_{165}$, $VEGF_{189}$ and $VEGF_{206}$). The isoforms result from different splicing events, and all variants share the same 115 N-terminal as well as six C-terminal residues [10,11]. $VEGF_{165}$ is the dominant isoform, while $VEGF_{206}$ has so far only been identified in a human fetal liver cDNA library [10]. $VEGF_{165}$ and $VEGF_{189}$ bind heparin with high affinity, and are sequestered to the cell surface or within the extracellular matrix bound to proteoglycans, while $VEGF_{121}$ does not bind heparin and is thus freely diffusible. Plasmin cleavage of $VEGF_{165}$ generates a 110-residue long N-terminal fragment (the receptor-binding domain) that no longer binds heparin but is equipotent to $VEGF_{121}$ in its ability to induce endothelial cell proliferation [12]. Therefore, the bioavailability of VEGF, in addition to the control of gene expression, might be triggered by proteolytic cleavage of the longer isoforms of VEGF [2] bound to heparan sulfate proteoglycan [12].

The receptor-binding domain of VEGF shares significant sequence homology with platelet-derived growth factor (PDGF) [13,14]. Recently, a number of growth factors were discovered that share higher sequence homology with VEGF than PDGF, some of which bind to identical receptors, namely placenta growth factor (PLGF) [15], VEGF-B [16] and VEGF-C (also named VEGF-related protein [VRP]) [17,18]. Not much is yet known about the specific biological roles of these homologs, but VEGF-C appears to be a growth factor specific for the lymphatic vascular system [19]. Of the two known receptor tyrosine kinases that bind VEGF, KDR/Flk-1 (human/murine homolog) and Flt-1, Flt-1 has the higher affinity for VEGF (K_D = 10–20 pM [20] compared to 75–125 pM for the KDR/Flk-1 receptor [21]); binding of VEGF to the KDR/Flk-1 receptor alone has been proposed to induce endothelial cell proliferation [22]. PLGF binds to the Flt-1 receptor with high affinity but not to KDR/Flk-1 [23]. VEGF-C binds to a third receptor tyrosine kinase called Flt-4 [24], which is not activated by VEGF [17]; whether or not VEGF-C binds to Flt-1 and KDR/Flk-1 remains controversial [17,18]. Although the VEGF binding epitopes for the KDR/Flk-1 and Flt-1 receptor have recently been determined [22,25], little is known at the molecular level about how specificity is achieved within this group of growth factors.

We have recently determined the crystal structure of a truncated construct of residues 8–109 of VEGF at 2.5 Å resolution [25,26]; the structure shows that VEGF is a member of the cystine knot growth factor superfamily. All members of this superfamily are dimeric growth factors, characterized by a cystine knot motif at one end of a conserved central four-stranded β sheet within each monomer (see [27–29]). The superfamily can be subdivided into four distinct families on the basis of sequence homology. Of the PDGF family, structures are known for PDGF-BB [30] and VEGF. In the transforming growth factor (TGF)-β family, structures have been determined for TGF-β1, -β2 and -β3 [31–34], osteogenic protein 1 [35], and glial cell-line derived neurotrophic factor (GDNF) [36], while nerve growth factor (NGF) is characteristic of the neurotrophins [37,38]. In contrast to the homodimeric dimerization observed for the native members of these first three families, the structure of human chorionic gonadotropin, a member of the fourth family, reveals a heterodimeric molecule [39,40]. Each of the homodimeric families shows a distinct dimerization mode. In VEGF and PDGF the two monomers are placed in a 'side-by-side' orientation linked by two disulfide bridges, and the twofold axis is perpendicular to the planes of the β sheets. In both the TGF-β and NGF families the β sheets of the two monomers are oriented in a 'face-to-face' orientation, but in NGF the twofold axis relating the two monomers is parallel to the strands, whereas in the TGF-β family it is perpendicular; there are no intersubunit disulfide bridges in NGF, while the TGF-β monomers are disulfide-linked.

Here we present the 1.9 Å crystal structure of human VEGF in a triclinic crystal form containing eight independent monomers in the asymmetric unit. The crystal structure shows that the eight monomers resemble a typical solution ensemble of protein structures, as determined by nuclear magnetic resonance (NMR) spectroscopy: a rigid core is surrounded by more variable loops. In the crystal structure these loops are associated with higher than average temperature factors. In contrast to the general 'random' variation in these loop conformations, for one of the loops the eight observed conformations describe a concerted movement, which we believe represents the motion of this segment in solution. Mapping mutational data onto the structure of VEGF reveals that this loop is implicated in binding to KDR/Flk-1 as well as to the Flt-1 receptor. These data suggest that this loop may be an important determinant of specificity within the group of VEGF-like growth factors, and that its flexibility in VEGF might be necessary for achieving promiscuity in binding to both KDR and Flt-1.

Results

Accuracy of the model

The structure of the receptor-binding domain of human VEGF was solved by molecular replacement (MR) and refined to a crystallographic R value of 20.9% (R free = 27.2%) for all reflections in the resolution shell between 16 and 1.93 Å (Figure 1; Table 1). The P1 unit cell contains eight VEGF molecules, which form four biological homodimers. All eight molecules (named A to H) are defined by continuous electron density. The crystallized fragment of VEGF consisted of residues 8–109, but only residues 14–106 are well defined in all eight monomers. In six molecules, one additional N-terminal and one additional

Figure 1

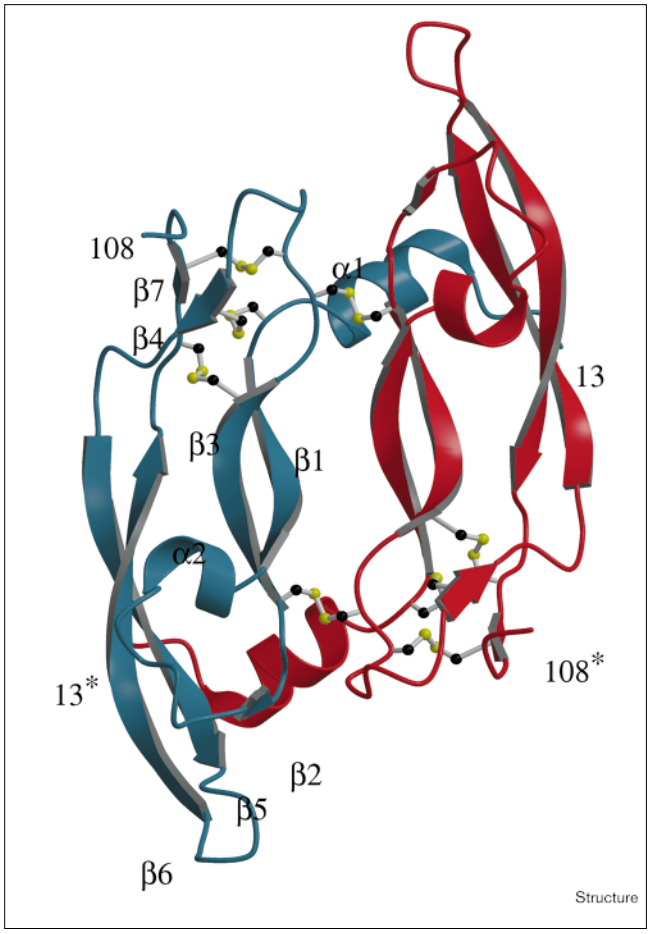

Ribbon representation of the structure of the receptor-binding domain of VEGF. The secondary structure elements of one monomer are labeled: α1 (residues 16–24), β1 (27–34), α2 (35–39), β2 (46–48), β3 (51–58), β4 (67–69), β5 (73–83), β6 (89–99) and β7 (103–105). One monomer of the dimer is shown in blue and the other in red; disulfide bonds are shown in white and sulfur atoms are in yellow. The termini of both monomers are labeled; the asterisks denote the termini of the red monomer. (The figure was prepared with the programs MOLSCRIPT [65] and RASTER3D [66].)

C-terminal residue are visible, and monomer A also includes residues 108 and 109. Glu13 and Asp109, when present, lack density for the sidechain and are modeled as alanine. The coordinate error of the final model, as deduced from a Sigmaa plot [41], is about 0.19 Å. Of all the residues, 90.3% have mainchain torsion angles in the most favorable regions of the Ramachandran plot (Figure 2), as defined from a statistical compilation of high-resolution structures [42], and no residues are located in disallowed regions. The root mean square (rms) deviation from ideal geometry of the final model is 0.011 Å for bond lengths and 0.030 Å for bond angle distances.

The average temperature factor of the final model is 47.1 Å^2 (Table 1). This is almost identical to the average temperature factor of 46.8 Å^2 observed in the 2.5 Å structure of VEGF in space group $P2_1$ [25]. The average temperature factors of the individual monomers vary from 41.3 Å^2 to 52.8 Å^2, and in general molecules belonging to the same dimer exhibit similar overall temperature factors. The exception is the dimer formed by molecules G and H, where the average temperature factors are 52.8 Å^2 and 43.8 Å^2, respectively. This difference may be caused by the difference in the extent to which these monomers participate in crystal-packing contacts, the mobility of molecule H in the crystal lattice being restricted by an additional 400 Å^2 of buried accessible surface area when compared to molecule G (see below). Val20 and Ser24 showed hints of alternative conformations in the final $(2F_o–F_c)\exp(i\alpha_c)$ electron-density map, but no alternative conformations were included in the model.

Table 1

Refinement and model statistics.

Model	
Total number of residues	762
Number of molecules (chains A to H)	8
Number of solvent molecules	640
Total nonhydrogen atoms	6782
Average B factor (Å^2)	47.1
Average B factor	
molecules A, B, C, D (Å^2)	41.3, 43.8, 50.0, 52.1
molecules E, F, G, H (Å^2)	43.1, 47.0, 52.8, 43.8
Average B factor of solvent molecules (Å^2)	52.1
Diffraction agreement	
Resolution (Å)	16.0–1.93
Completeness (%)	94.2
R value (all data)	0.209
Number of reflections	61 827
Free R value	0.272
Number of reflections	7074
Anisotropic correction (Å^2)	14.0
Stereochemistry	
Rms difference in bond distance (Å)*	0.011
Rms difference in angle distance (Å)*	0.030
Rms ΔB of bonded atoms*	
mainchain (Å^2)	2.0
sidechain (Å^2)	2.5

*Rms = root mean square.

Monomer structure

The overall structure of the VEGF monomer is similar to that of other cystine knot proteins [27–29,43]. It consists of a central antiparallel four-stranded β sheet with the characteristic cystine knot at one end (Figure 1). The cystine knot consists of two disulfide bonds forming a covalently linked ring structure between two adjacent β strands (β3 and β7), together with a third disulfide bond penetrating this ring and connecting the beginning of strands β1 and β4 (Figures 3 and 4a). In NGF a loose ring is formed by a total of 14 residues, while in all other members of the superfamily a tighter ring is formed by eight residues. This tight ring

Figure 2

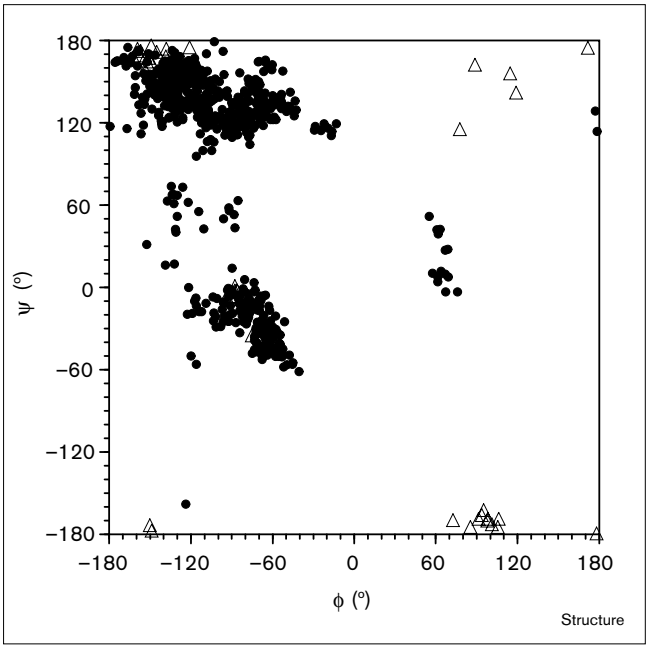

Ramachandran representation of the mainchain dihedral angles of all residues in the asymmetric unit. Glycine residues are indicated by triangles, all other residues by dots. According to a statistical compilation of high-resolution structures [42], 90.3% of all non-glycine residues are located within the most favored regions, 0.8% in generously allowed regions, and none in the disallowed regions of the Ramachandran space.

is characterized by the strict conservation of a glycine residue (position 59 in VEGF; Figure 3) due to a potential clash between any sidechain at this position and the knot. In addition, Gly59 is required to have a positive dihedral ϕ angle (the average ϕ,ψ values of Gly59 in VEGF are $97.8 \pm 6.3°$ and $-169.5 \pm 3.9°$, respectively).

A detailed analysis of the mainchain hydrogen bonds in VEGF reveals a total of seven β-strand segments (β1 to β7) and two α-helical segments (α1 and α2) (Figures 1 and 3). The central four-stranded β sheet can be divided into two separate pairs of β strands (β1 and β3; β5 and β6); only a single mainchain hydrogen bond is formed between Met55 and His99 of the two inner strands (Figure 3). In addition to the lack of regular hydrogen bonding at the center of the sheet, the β sheet is solvent-exposed from both sides (Figure 1). Therefore, the cystine knot is probably important for the stabilization of the fold (Figure 4a). Interestingly, a second hydrophobic core is formed across the monomer–monomer subunit interface at the opposite end of the monomer to the knot (Figure 4b). Residues involved in this hydrophobic core are from loop β1 to β3 and segment β5 to β6 of one monomer, and the N-terminal α helix of the other monomer. The lack of an extended hydrophobic core at the center of the molecule in both the monomer and the dimer might be the reason for the high chain mobility as expressed by the high overall temperature factor of the model.

In the case of NGF it has been suggested that cystine knot proteins exhibit a more pronounced twist within the β strands than other proteins [37]. However, although β1 and β3 both contain proline residues, whose dihedral ϕ angle values are restrained to significantly higher values than in regular β strands, the average ϕ,ψ values of the strand residues ($\phi = -109.4 \pm 35.1°$, $\psi = 136.0 \pm 32.4°$) are comparable to those observed in α–β proteins [44]. A similar result is observed for the average dihedral angles of residues from strands β5 and β6 ($\phi = -116.5.4 \pm 23.3°$, $\psi = 139.0 \pm 28.1°$). Within these assumed strand limits, therefore, the β strands in VEGF do not deviate from the regular right-handed twist.

Each VEGF monomer contains three solvent-accessible loop regions, namely the loops connecting strand β1 to β3, β3 to β4, and β5 to β6. The segment connecting strands β1 and β3 (residues 35–50) contains a single turn of α helix (α2), followed by residues in an irregular conformation and a short segment of β-strand structure (β2). This short β strand together with neighboring strands β5 and β6 forms a short, three-stranded antiparallel β sheet at the opposite end of the monomer to the cystine knot (Figure 3), and has been shown to be part of the receptor-binding face of VEGF [25].

Loop β3 to β4 is adjacent to the cystine knot and differs greatly in length between different cystine knot proteins, but is similar in length in VEGF and PDGF. Residues in the loop regions together with the N- and C-terminal residues display the highest temperature factors in the VEGF structure.

Dimer structure

The different cystine knot proteins have similar monomer topologies but differ greatly in the way the dimers are formed [27]. VEGF and PDGF dimerize in an antiparallel, side-by-side fashion [25,30] (Figures 1 and 3). In VEGF the monomers are covalently linked by two symmetrical disulfide bonds between Cys51 and Cys60. No mainchain to mainchain hydrogen bonds are formed between the two neighboring strands β1 and β1′ of the two subunits; the only intersubunit mainchain hydrogen bonds are found between Val15 of the N terminus and Thr77′ and Gln79′ of the outer β strand β5 (Figure 3). At the location of the dimer axis, four water molecules are conserved in all four independent dimers within the crystals.

The total area buried at the interface between the two subunits is 2695 ± 28 Å^2. Most of this (1730 Å^2, or 65% of the total) is accounted for by the intermolecular hydrophobic core located at the opposite end of the molecule to

Figure 3

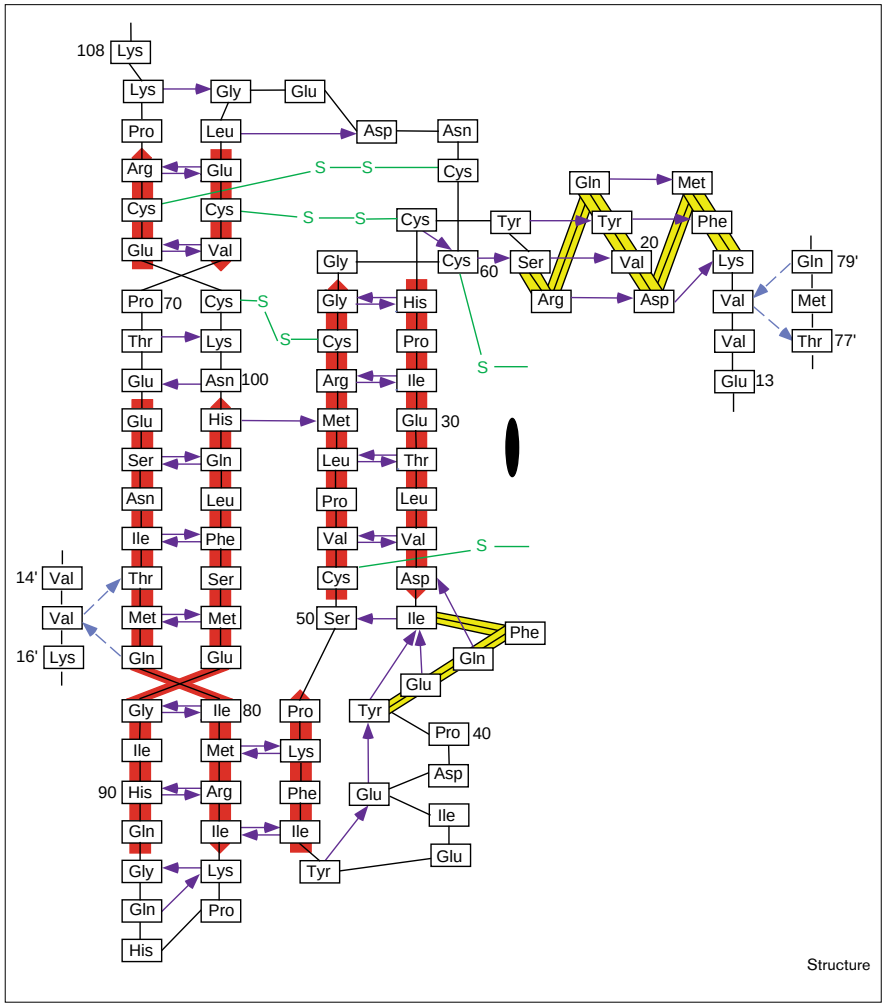

VEGF secondary structure, showing the mainchain hydrogen-bond pattern observed within the monomer. Disulfide bridges are shown in green and the twofold axis of the dimer is indicated by a black ellipse. β Strands are shown in red, helical segments in yellow. All mainchain hydrogen bonds are indicated by blue arrows (direction: hydrogen-bond donor (N-H) to hydrogen-bond acceptor (O)). A distance cut-off of 3.5 Å was used; when several hydrogen bonds are possible only the shortest is shown. The mainchain hydrogen bonds are very strictly conserved within the eight monomers in the asymmetric unit, and ambiguity is only observed at the capping of the helices. For example, in two monomers the mainchain hydrogen-bond distance between Tyr25 and Gln22 (residues i and i+3) is shorter than that between Tyr25 and Tyr21 (residues i and i+4). With the exception of the absence of the mainchain hydrogen bond between Lys84 and Gly88 in one monomer, all mainchain hydrogen bonds between β strands are strictly conserved in all eight monomers. Only two mainchain hydrogen bonds are formed between monomers within the dimer. These are the bonds between the N-terminal residue Val15 of one monomer and Thr77 and Gln79 of the second monomer, and are indicated by broken lines. The single glycosylation site in VEGF is at Asn75 [67] near the beginning of strand β5.

the cystine knot, consistent with the observation that there are only a few contacts between the β1 strands of the two subunits at the center of the dimer. Interestingly, this hydrophobic core region, containing the most extensive contacts within the dimer (Figure 4b), is also part of the receptor-binding site which extends across the subunit interface [25] (see below).

Solvent structure and crystal packing

The current model includes a total of 640 water molecules for 762 ordered protein residues. Assigning each water molecule to individual monomers in the asymmetric unit yields 117, 90, 58, 65, 97, 74, 54 and 91 water molecules for monomers A–H, respectively (six water molecules are counted twice because their assignment was ambiguous). Each water position was further inspected for conservation within the different monomers. By applying a 1 Å distance cut-off after superposition of the monomers, a total of 72 water molecules were found to be present in all eight monomers, occupying nine conserved positions. In addition, 49, 42, 60, 56, 66 and 88 water molecules were conserved in seven, six, five, four, three and two monomers, respectively; 207 waters were only observed once.

As a consequence of the lack of space group symmetry, each monomer has a different crystallographic environment, which results in significantly different crystal-packing contacts. The area of each monomer buried in crystal-packing contacts (omitting the monomer–monomer contact of the biological dimer) is 1270, 1530, 1140, 1100, 1330, 1210, 1220 and 1650 Å^2 for monomers A to H, respectively. Thus, about 20 to 30% of the total 5710 Å^2 monomer accessible surface in the dimer is buried in crystal-packing contacts, a range typical for protein crystals [45,46]. One contact occurs several times. This contact involves a local twofold axis and packs loops β5 to β6 and α2 to β3 of one monomer against loop β3 to β4 of a second monomer, and vice versa. This contact is quite extensive (~430 Å^2) and includes a pi-stacking interaction between the aromatic sidechains of Phe36 and His86 (data not shown).

Figure 4

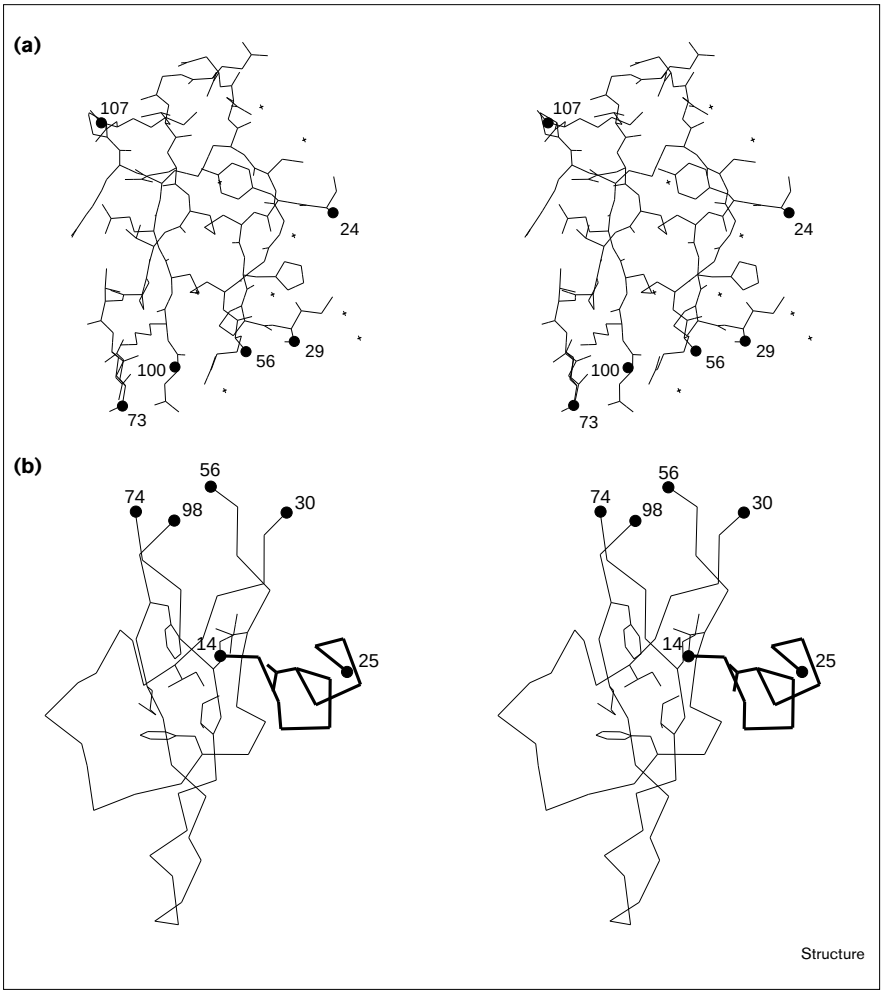

Structural details of VEGF. **(a)** Stereo representation of all atoms within the cystine knot. Water molecules are shown as crosses if present at equivalent positions in all eight monomers. **(b)** Stereo representation showing the hydrophobic core formed at the opposite end to the cystine knot and extending across the monomer–monomer interface. Residues whose sidechains contribute to this hydrophobic core are Ile35, Phe47, Val52, Met78, Ile80, Met94, Phe96 of one monomer (thin lines) and Val20 of helix α1 from the second monomer (bold lines). Ends of segments of the mainchain are indicated by small spheres.

Discussion

Comparison with PDGF and other cystine knot proteins

The three-dimensional structures of a number of cystine knot growth factors have been solved in recent years and the structures have been reviewed [27–29,43]. The members of this superfamily exhibit similar monomer structures but differ in their dimerization mode. As predicted on the basis of sequence alignments, the dimerization mode of VEGF is very similar to that of PDGF-BB. The monomers of VEGF can be superimposed onto PDGF-BB with an rms deviation of 1.7 Å (using 73 Cα atoms, a distance cut-off of 3.8 Å, and the program O [47]); superimposing the dimers yields an rms deviation of 1.9 Å (for 124 Cα atoms), indicating that the relative orientation of the monomers within the dimer is indeed very similar in both growth factors (Figure 5a).

There are three major differences between VEGF and PDGF-BB, and it is noteworthy that these differences all involve regions important for receptor binding. The N-terminal segment, which lies across the four-stranded β sheet of the second monomer, is α helical in VEGF but forms an extended conformation in PDGF-BB. In VEGF, this N-terminal α helix forms part of the receptor-binding face, and mutagenesis has shown that Phe17 from this helix is an important KDR-binding determinant [25]. To our knowledge no residues in the extended N terminus of PDGF have thus far been tested for receptor binding, but it is tempting to propose that the difference in conformation of this segment near the N terminus is important for receptor specificity. The segment connecting strands β1 and β3 in VEGF (residues 35–50) is not resolved in the structure of PDGF-BB, but sequence alignment shows this loop is two residues longer in PDGF (see below). Residues from this segment have been implicated in receptor binding in both VEGF [25] and PDGF [30]; in VEGF the segment contains a single helical turn (α2 in Figure 1) followed by residues in an irregular conformation. It is noteworthy that the conformation of this segment is similar to that observed in members of the

Figure 5

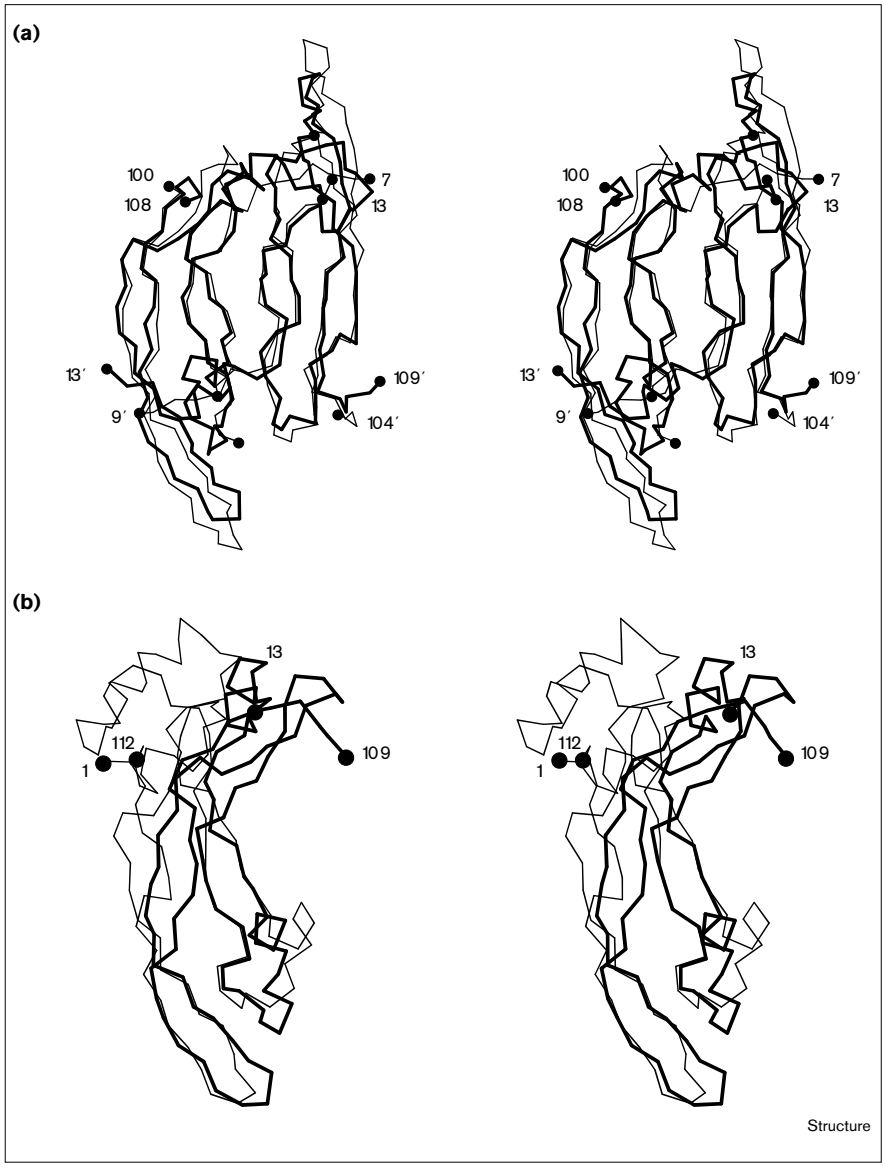

Comparison of VEGF with other cystine knot growth factors. **(a)** Stereo representation of the superposition of the structures of VEGF and PDGF-BB. VEGF is shown in bold lines and PDGF-BB (PDB entry code 1PDG) in thin lines. The structures can be superimposed with an rms deviation of 1.9 Å for 124 Cα atoms (distance cut-off 3.8 Å, program O [47]). **(b)** Superposition of the structures of VEGF (bold lines) and TGF-β2 (thin lines; PDB entry code 2TGI). Both growth factors were superimposed using residues from the opposite end of the molecule to the cystine knot (rms deviation: 2.1 Å for 44 Cα positions). The superposition suggests that a structurally conserved receptor-binding frame is responsible for receptor recognition in both VEGF and TGF-β (see text). The ends of mainchain segments are indicated with small spheres.

TGF-β family (see below). The third major difference between VEGF and PDGF is a three-residue deletion in VEGF at turn β5–β6; this is also likely to have implications for receptor specificity because residues adjacent to this turn are involved in receptor binding (see below).

Most of the previous comparisons between more distantly-related members of the cystine knot superfamily were based on the superposition of the knot itself. The surprising similarity between VEGF and TGF-β in the segment connecting β1 to β3 prompted us to superimpose the opposite ends of the monomers (Figure 5b). This superposition yields an rms difference of 2.1 Å for 44 atoms, compared to 1.4 Å for 38 atoms when superimposing the cystine knot (distance cut-off = 3.8 Å). The superposition shows that in addition to helix α2, strand β2 is also conserved in both growth factors, resulting in a very similar, short three-stranded β sheet at the end of the molecule opposite to the knot. This three-stranded β sheet is involved in receptor binding in VEGF [25], and this same region (although on the opposite face of the sheet) has been proposed to bind to one of the TGF-β receptors [48]. Recently, a ligand which might mimic the binding of proteoglycans has been found to bind to this face in TGF-β3 [34].

Eight copies of VEGF

The crystal structure of VEGF (residues 8–109) contains eight copies of the monomer in the asymmetric unit.

Figure 6

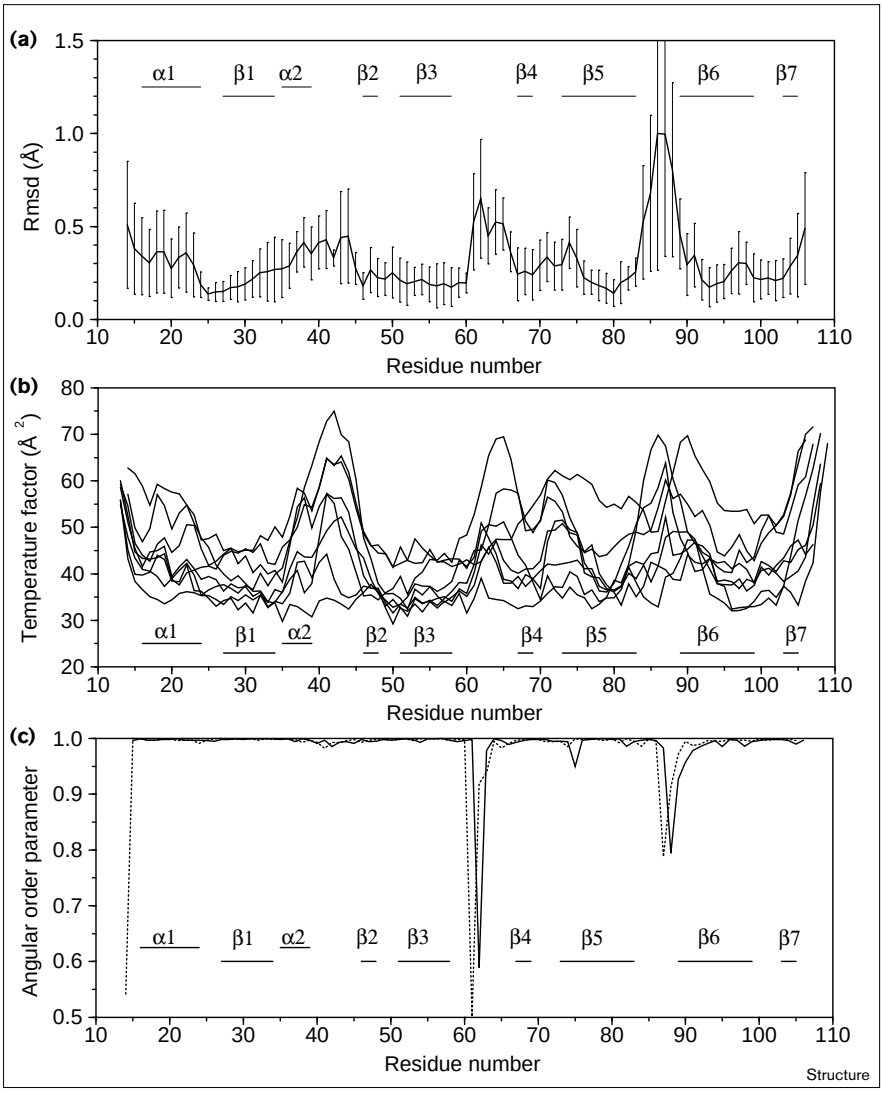

Comparison of the eight copies of VEGF. **(a)** Average distance deviation per residue from the geometrically averaged structure calculated following best-fit superposition of the mainchain atoms of residues 16–24, 27–39, 46–48, 51–58, 67–69, 73–83, 89–99 and 103–105. Vertical error bars indicate the rms difference from the average within the eight monomers. Secondary structure elements are indicated by horizontal lines. **(b)** Average mainchain temperature factors per residue for all eight monomers. **(c)** Angular order parameter plot. The angular order parameter is defined as the normalized vector sum of the mainchain dihedral angles observed in the different copies of VEGF (ϕ order parameter, continuous line; ψ order parameter, dotted line). The decrease in the angular order parameter at the peptide-bond between residues 61 and 62 results from a peptide-bond flip (six monomers in one conformation, and two in the other).

This unusually high number of independent molecules allows a discussion of protein flexibility observed in crystals through methods analogous to those used for solution structures determined by NMR techniques. The average rms difference for the mainchain atoms (N, Cα, C and O) with respect to the mean coordinates and calculated for secondary structure elements only is 0.24 ± 0.06 Å (Figure 6a); when all atoms of these same residues are used, this number increases to 0.37 ± 0.11 Å. As expected, the eight molecules are very similar in the core region of the molecule. The greatest deviations are found in loop segments β1 to β2, β3 to β4 and β5 to β6, as well as in the N-terminal α helix (Figure 6a). All these regions are well defined by their density. In all eight molecules, residues from or near the loop regions are involved in crystal-packing contacts; it is noteworthy that NMR experiments have shown flexibility in the middle of helix α1 [49]. The rms deviations among the eight copies are similar to the deviations derived by NMR from the highest-precision ensembles, showing that a precision comparable to high-resolution X-ray structures can be achieved by NMR.

The increased conformational diversity in loop regions correlates well with the increase in temperature factors within the same segments when compared to the low deviations in the core regions of the molecule (strands β1, β3, β5 and β6) (Figure 6b). Outside the loop regions, the temperature factors also show a significant increase at residues 71–74. These residues connect strand β4 to β5, and the increase might reflect higher flexibility made possible by the lack of regular β strand hydrogen bonding between these residues and the neighboring strand (Figure 3). Despite the higher temperature factors, the increase in the rms differences at these residues is less pronounced.

Figure 7

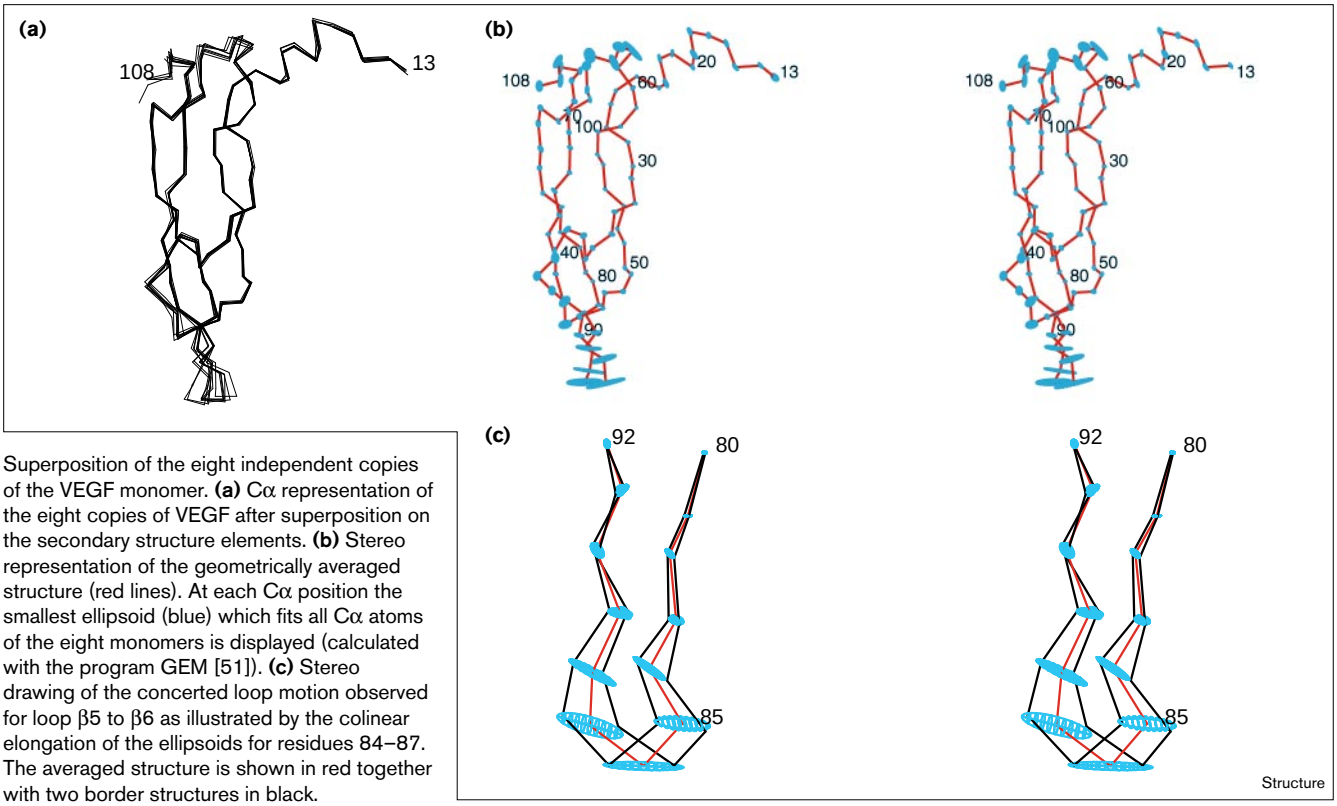

Superposition of the eight independent copies of the VEGF monomer. **(a)** Cα representation of the eight copies of VEGF after superposition on the secondary structure elements. **(b)** Stereo representation of the geometrically averaged structure (red lines). At each Cα position the smallest ellipsoid (blue) which fits all Cα atoms of the eight monomers is displayed (calculated with the program GEM [51]). **(c)** Stereo drawing of the concerted loop motion observed for loop β5 to β6 as illustrated by the colinear elongation of the ellipsoids for residues 84–87. The averaged structure is shown in red together with two border structures in black.

The angular order parameter plot for ϕ and ψ [50] emphasizes the conservation of the dihedral conformation within the eight copies of VEGF (Figure 6c). The average ϕ and ψ order parameters are 0.987 ± 0.048 and 0.981 ± 0.073, respectively. The most severe decrease in the order parameter is observed for the peptide bond between residues 61 and 62 in loop β3 to β4, and results from a partial peptide flip. The order parameter is also much lower for residues 87 and 88 in loop β5 to β6. Interestingly, the largest reduction within this loop is not observed at the tip of the loop but for residues adjacent to the loop, namely at the beginning of strand β6. A small but significant reduction is also observed for residues at the end of strand β5.

It has been shown that although crystal-packing contacts induce conformational diversity, the conformations 'frozen' within the crystals represent true low-energy conformations [46]. We decided to study in more detail the conformational diversity observed in the N-terminal α helix and the three exposed loop segments β1 to β2, β3 to β4 and β5 to β6, as well as the C terminus. After superposition of the mainchain atoms (Figure 7a), we calculated the smallest possible ellipsoid containing all Cα positions of the same residues observed in the eight monomers with the program GEM [51], and displayed the ellipsoids in program O [47] (Figure 7b). In all but one of the loops as well as in the N-terminal α helix, no concerted displacement is observed. In loop β5 to β6, however, the observed atomic positions of the eight monomers represent different snapshots of a concerted loop movement, yielding displacements as large as 4.7 Å at the tip (His86). The loop itself retains its conformation (Figures 7b,c), whereas residues next to the loop serve as hinges, in good agreement with the angular order parameter plot.

TGF-β1 is the only member of the cystine knot superfamily whose structure has been determined in solution using NMR techniques [32]. As the structures of the TGF-β1 and VEGF monomers are very similar, it is possible to compare the conformational variability of TGF-β1 in solution with the ensemble of eight structures observed in the crystal of VEGF. Both structures are of good quality, as judged by a high number of restraints and high resolution, respectively. In the TGF-β1 dimer, the rms difference of the backbone relative to the mean is 0.71 Å when some loops are excluded; this high deviation is attributed to a hinge movement at the center of its four-stranded β sheet [32]. Based on a simulation of a distance restraint refinement using the coordinates from the crystal structure of TGF-β2 as a starting model, the authors conclude that this large hinge movement is due to the absence of long range restraints and therefore an artifact of the refinement. The

Figure 8

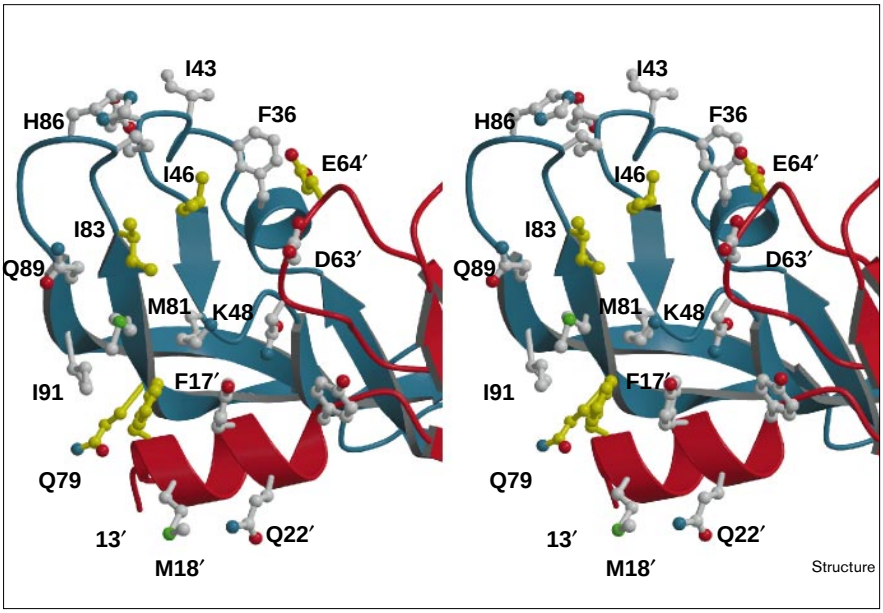

Stereo representation of the receptor-binding face of VEGF. The receptor-binding face is built from strands β2, β5 and β6 from the first monomer (blue) and helix α1 from the second monomer (red) as well as adjacent loops. This view of the molecule is generated from Figure 1 by an approximately 90° rotation around a horizontal axis in the plane of the paper. The most important binding determinants for the KDR receptor, as identified by mutagenesis [25], form two hot spots: Phe17′ and Gln79; and Ile46, Glu64′ and Ile83 (shown in yellow). We propose that residues accessible on the same face (shown in gray) are responsible for receptor-binding specificity among VEGF and its homologs. For example, a limited number of residues (namely Asp63′, Glu64′ and Glu67′) have been identified to participate in binding of VEGF to its Flt-1 receptor [22]. Glu67′ is part of the loop containing Asp63′ and Glu64′, and all three residues are exposed on the receptor-binding face. (The figure was drawn with the programs MOLSCRIPT [65] and RASTER3D [66].)

recent crystal structure of GDNF [36], however, shows precisely such hinge variation between the two dimers in the asymmetric unit, thus, hinge movement may be a contributing factor to the high rms deviations observed in TGF-β1. Such hinge motion is not observed for VEGF or PDGF, probably due to the difference in dimerization mode.

Considering the monomer only, superimposing the first 17 structures of TGF-β1 (Brookhaven Protein Data Bank entry code 1kla; monomer A) based on the N, Cα, C and O atoms in the β strands and helix α2 gives an rms difference from the mean coordinates of 0.32 ± 0.09 Å, which is comparable to the difference calculated for our eight VEGF monomers. Through the use of ^{15}N relaxation experiments the authors identify only a single segment in the finger region of TGF-β1 that shows significant local flexibility on a picosecond time scale in solution. This segment is equivalent to the tip of loop β5 to β6 in VEGF and is limited to about eight residues. Interestingly, these are the very residues to which we attribute a concerted loop movement based on our analysis of the independent monomers in our crystals (Figure 7c). Overall, the comparison of these two cystine knot proteins yields a surprisingly good correlation in the conformational flexibility of the molecules in the crystal versus solution.

Receptor binding

VEGF binds to two different receptors: the KDR/Flk-1 receptor and the Flt-1 receptor. The extracellular portion of both receptors consists of seven IgG-like domains, and the receptors share 44% homology [2]. Charge reversal and alanine scanning mutagenesis have allowed identification of the receptor-binding epitope of VEGF for KDR/Flk-1 [22,25]. Five residues were found to contribute most of the binding energy. These five residues (Phe17, Ile46, Glu64, Gln79 and Ile83) are clustered into two different patches, each of which extends across the VEGF dimer interface (Figure 8). All five residues are located on one face of the VEGF dimer, which we refer to as the receptor-binding face. This face consists of the short three-stranded β sheet (strands β2, β5 and β6) and loop β1 to β2 of one monomer together with the N-terminal α helix and loop β3 to β4 of the second monomer. In PDGF, the residues that have thus far been implicated in receptor binding all map on the equivalent face [30,52,53].

The VEGF homologs PLGF, VEGF-B and VEGF-C, differ in their ability to bind to different receptors. PLGF only binds to Flt-1 and not to KDR [21]. Sequence alignments show that of the five most important KDR-binding determinants of VEGF, four are totally conserved between VEGF and PLGF, while the fifth residue is changed from isoleucine to methionine (Figure 9). Ile46 is one of three residues that contribute most to the KDR-binding energy [25], and this single difference is likely to significantly affect the affinity for KDR. However, other residues closeby and displayed on the same binding face are also likely to contribute to the changes in specificity. Non-conservative differences in these residues are Met18→Gln, Gln22→Gly, Lys48→Ser, Asn62→Gly, Gly65→Asn, Pro85→Ser, His86→Gly and Gln89→Pro. Of particular interest are the differences in residues 85, 86 and 89 in the loop connecting β5 to β6: these changes, involving two prolines and a glycine, are likely to affect the observed movement of the

Figure 9

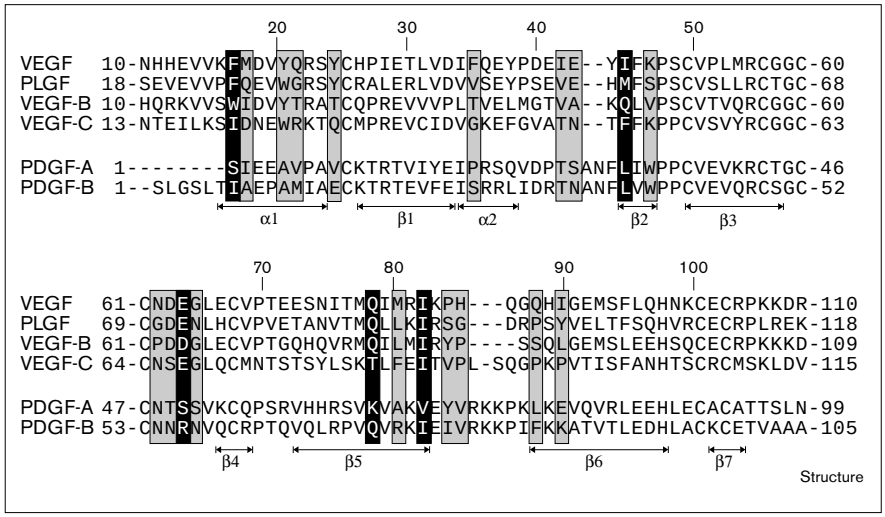

Sequence alignment of VEGF, PLGF, VEGF-B, VEGF-C, PDGF-A and PDGF-B. The secondary structure assignment in VEGF is shown by arrows. Black boxes identify the binding determinants of VEGF for the KDR receptor [25]. Gray boxes identify residues accessible on the same receptor-binding face as the KDR-binding determinants in VEGF. Mutations in these residues might be responsible for differences in affinity and selectivity within the VEGF group. Because of the structural similarity between VEGF and PDGF, and supported by the mutagenesis data published so far, the same positions might be responsible for receptor recognition by PDGF [30,52,53]. (The sequences of PLGF, VEGF-B, VEGF-C, PDGF-A and PDGF-B were obtained from the Swissprot databank with accession numbers P49763, P49765, P49769, P04085 and P01127, respectively.)

loop. We speculate that the expected change in loop flexibility might be an important contribution to receptor specificity. Other changes of interest are Asn62→Gly and Gly65→Asn, because they are located near Glu64, a critical binding determinant of VEGF for KDR. As Glu64 is also important for binding to Flt-1, it is unlikely that the differences at positions 62 and 65 result in gross local conformational changes, therefore, these residues might be involved in direct receptor contacts.

Although VEGF-C stimulates the autophosphorylation of the KDR receptor [17], unlike VEGF it is not possible to coprecipitate VEGF-C with a KDR–IgG fusion protein, suggesting that the interaction of VEGF-C and KDR is weak [18]. Of the five residues important for binding of VEGF to KDR, only Glu64 and Ile83 are present in VEGF-C (Figure 9). The differences in the remaining four residues may suffice to explain the weakened binding between VEGF-C and KDR, and it would be interesting to test the importance of these four residues using mutagenesis.

VEGF binding to the Flt-1 receptor appears to be mostly mediated through loop β3 to β4 [22]. Of all single alanine substitutions tried, only those at Asp63 and Glu64, which are both located in this loop, were found to significantly reduce affinity in a direct binding assay, without, however, accounting for the entire binding energy [22]. These residues are conserved in VEGF and PLGF, while in VEGF-C, which does not bind to Flt-1, Asp63 is changed to serine (Figure 9). This suggests that position 63 is important for specificity.

Sequence alignments show that the Flt-1 receptor is expected to be structurally similar to the KDR/Flk-1 receptor [2]. We believe, therefore, that VEGF binds in a similar manner to both receptors. This is analogous to the binding of human growth hormone to both the growth hormone receptor and the prolactin receptor, for which extensive mutagenesis and structural data are available [54–56]. The crystal structures of these complexes reveal that although significant differences are found in detail, the overall arrangement of receptor and hormone is surprisingly similar, and in both complexes the same set of residues is buried at the interface. Even so, the relative importance of the individual contact residues is different for binding to the growth hormone or the prolactin receptor. Therefore, receptor specificity can be achieved by residues different from those contributing most to the binding energy, thus decoupling binding and specificity determinants [56]. We believe similar mechanisms operate for the receptor binding of VEGF, PLGF and VEGF-C, and it will be interesting to gain structural insights into how these homologous growth factors bind to their receptors and how specificity is achieved in each case.

Biological implications

Vascular endothelial growth factor (VEGF) is a highly specific mitogen promoting the formation of blood vessels in embryogenesis and wound healing. It is also involved in pathological angiogenesis such as tumor growth, diabetic retinopathy, and rheumatoid arthritis. These biological properties make VEGF an important therapeutic target, and it has been shown that anti-VEGF antibodies can inhibit tumor growth *in vivo*. At the molecular level, VEGF activity is mediated by its interaction with two distinct receptors, KDR and Flt-1. A detailed structural and functional characterization of the interactions between VEGF and its receptors is a prerequisite for the design of small-molecule antagonists.

The crystal structure of the receptor-binding domain of VEGF shows that it is a member of the cystine knot growth factor superfamily. A comprehensive mutagenesis analysis has revealed that the residues important for KDR binding map in two patches on the same face of the molecule, spanning across the dimer interface. The main structural feature of this receptor-binding face is a short three-stranded, antiparallel β sheet in one subunit, which packs against the N-terminal α helix from the other subunit. This interaction accounts for 65% of the total surface buried within the dimer, and may be important for the stability of the receptor-binding face.

Analysis of the conformational variability of VEGF shows that the loop connecting strand β5 to β6 undergoes a concerted movement. This loop is important for binding to both KDR and Flt-1, therefore, the flexibility of the loop might be functionally important in accessing different conformations required for binding to these distinct receptors. Although the role of the VEGF homologs, placenta growth factor (PLGF), VEGF-B and VEGF-C, in the regulation of angiogenesis is still poorly understood, multiple sequence alignment helps to explain at an atomic level the differences in specificity of the VEGF homologs towards KDR and Flt-1.

Compared to other cystine knot growth factors, VEGF shows greatest structural similarity to platelet-derived growth factor (PDGF). Three major differences are observed between VEGF and PDGF, all in regions important for receptor binding. A comparison of VEGF with the structure of transforming growth factor (TGF)-β reveals greater similarity than previously expected, because a loop region that was missing in PDGF has a conformation very similar to the analogous segment in TGF-β; the similarity extends to the region identified as the receptor-binding face in VEGF. This structural conservation suggests functional conservation, consistent with limited mutagenesis data implicating this same region of the monomers in PDGF and TGF-β for receptor binding.

Materials and methods

Crystallization and data collection

A construct consisting of residues 8–109 of human VEGF was expressed, refolded and purified as described [26]. Triclinic crystals (P1, a = 45.5 Å, b = 68.5 Å, c = 85.8 Å, α = 105.4°, β = 93.71°, γ = 101.49°) were grown from large sitting drops obtained by mixing 40 μl of protein solution (15 mg/ml protein in 20 mM Tris-HCl, pH 7.5, 0.4 M sodium chloride) with 40 μl of reservoir solution (14% PEG 3350, 10% isopropanol, 0.2 M ammonium acetate pH 5.6), and equilibrating against 30 ml of reservoir solution. Crystals grew to a typical size of $600 \times 80 \times 80$ μm within four weeks. The crystals could be flash-frozen directly from the drops, after increasing the isopropanol content of the reservoir to 20% and equilibrating against the altered reservoir for one week. (At the end of this period the crystals started to disintegrate and monoclinic crystals appeared spontaneously. Similar monoclinic crystals directly grown from high isopropanol conditions were previously used to determine the structure of VEGF by multiple isomorphous replacement methods (MIR) [25]).

A complete data set to 1.9 Å was collected from a single flash-frozen crystal on beamline F1 (λ = 0.909 Å) at the Cornell High Energy Synchrotron Source equipped with the Princeton CCD-detector. Two sets of exposures, 184 images of 1° oscillation at a detector–crystal distance of 80 mm and 91 images of 2° oscillation at a distance of 120 mm, were processed independently with program DENZO, after which the two data sets were scaled together with program SCALEPACK [57]. A total of 180,803 observations was reduced to 72,050 unique reflections, with an overall R_{merge} of 4.4% (12.7% between 2.0 and 1.9 Å resolution). The resulting data set was 94% complete in the resolution range between 20 and 1.90 Å (81% in the shell between 2.0 and 1.9 Å resolution).

Molecular replacement

The structure was solved by MR using the 2.5 Å structure of VEGF previously solved by MIR techniques in space group $P2_1$ as a search model [25], using a dimer with all atomic temperature factors set to 20 Å^2. The rotation function was calculated with the program XPLOR [58], using all reflections between 10 and 4 Å resolution and an integration sphere from 5 to 20 Å. After Patterson correlation refinement [59] of the first 200 solutions, during which the two monomers within the dimer were allowed independent adjustments, a set of eight solutions with correlation coefficients between 0.15 to 0.10 stood out clearly above the noise at 0.06. The eight rotation solutions represented the four VEGF dimers in the asymmetric unit, corresponding in a Matthews parameter [60] of 2.7 Å^3/Da.

The translation search was calculated with the program AMORE [61] using reflections between 20 and 4.0 Å resolution. The first dimer was arbitrarily positioned at the origin and an unambiguous solution was found for the second dimer, with an R value of 55.9% and a correlation of 15.6% (next position: R value = 57.6% and correlation coefficient = 10.8%). The subsequent translation search for the third and fourth dimers increased the correlation to 24.4% and 33.1%, while decreasing the R factor to 53% and 49.6%, respectively. Identical translation solutions were obtained when the order in which the rotated dimers were translated into the unit cell was permutated. Inspection of the model with the program O [47] revealed a convincing packing scheme and the absence of any stereochemical clashes. In addition, consistent with the correct space group assignment, each monomer has a unique crystallographic packing environment.

Refinement

Before refinement, 10% of all measured reflections were set apart for subsequent monitoring of the free R value [62]; these reflections were selected in 20 thin resolution shells to remove possible bias resulting from noncrystallographic symmetry. Rigid-body refinement of the MR model to 3 Å resolution resulted in an R value of 41.6% (free R value 44.1%). The model was subsequently refined by alternating a total of 24 rounds of conventional refinement using program XPLOR [58] with visual inspection and model building using the program O [47], while gradually increasing the resolution to 1.93 Å. After several rounds of refinement the native data set was corrected for observed anisotropy, the biggest difference of 14 Å^2 being observed between the a* and c* axes.

Initially, water positions were derived from peaks greater than 4σ in a Sigmaa-weighted [41] difference map; later 3.5σ peaks in a regular F_o–F_c density map were considered. After each refinement round, water molecules were removed if their temperature factors exceeded 80 Å^2 or displayed less than 1σ density in the resulting $2F_o$–F_c density map.

At this stage of the refinement the crystallographic R value had dropped to 20.9% for all reflections between 8 and 1.93 Å resolution, but the free R value was still as high as 31.1% and could not be further decreased through model rebuilding or incorporation of water molecules. To investigate possible overfitting of the data, two series of omit maps [63] were calculated: VEGF dimers were removed one by one, together with all solvent molecules, and the remaining model subjected to simulated annealing at 1000 K with the program XPLOR [58]; secondly, single

monomers were deleted one by one and the remaining structure refined against all data between 16 and 1.93 Å resolution using maximum likelihood refinement with the program REFMAC [64]. Inspection of the Sigmaa-weighted omit maps confirmed the correct placement of the VEGF molecules and allowed only for minor adjustments at the very terminal residues in the individual chains. After rebuilding, several rounds of refinement with REFMAC using a bulk-solvent correction and all data between 16 and 1.93 Å resolution resulted in a significant decrease from 3.9 to 2.0 $Å^2$ in the rms deviation of the temperature factors of bonded mainchain atoms. Prior to the last refinement round an explicit bulk-solvent mask was calculated with XPLOR [58] and introduced into REFMAC [64] using partial structure factors. Noncrystallographic symmetry restraints were gradually loosened throughout the refinement and removed completely near the end, resulting in a drop in both the free R value and the crystallographic R value of 0.9%. Refinement was halted after the R value dropped to 20.9% (free R value = 27.2%) and no interpretable difference density remained in the final $(F_o–F_c)\ \exp(i\alpha_c)$ electron-density map.

Accession numbers

The coordinates have been deposited in the Brookhaven Protein Data Bank for release on July 30, 1998; the accession code is 2VPF.

Acknowledgements

We thank Wayne Fairbrother for numerous scientific discussions, for doing ensemble rms difference and order parameter calculations, and for critical reading of the manuscript. We also thank the staff at CHESS for help with beamline F1, and Trissa Elkins, Charles Eigenbrot, and Mike Randal for help with data collection.

References

1. Folkman, J. (1995). Angiogenesis in cancer, vascular, rheumatoid and other disease. *Nat. Med.* **1**, 27–31.
2. Ferrara, N. (1995). The role of vascular endothelial growth factor in pathological angiogenesis. *Breast Cancer Res. Treat.* **36**, 127–137.
3. Dvorak, H.F., Brown, L.F., Detmar, M. & Dvorak, A.M. (1995). Vascular permeability factor/vascular endothelial growth factor, microvascular hyper-permeability and angiogenesis. *Am. J. Pathol.* **146**, 1029–1039.
4. Neufeld, G., Tessler, S., Gitay-Goren, H., Cohen, T. & Levi, B.Z. (1994). Vascular endothelial growth factor and its receptors. *Prog. Growth Factor Res.* **5**, 89–97.
5. Carmeliet, P., *et al*., & Andras, N. (1996). Abnormal blood vessel development and lethality in embryos lacking a single VEGF allele. *Nature* **380**, 435–439.
6. Ferrara, N., *et al*., & Moore, M.W. (1996). Heterozygous embryonic lethality induced by targeted inactivation of the VEGF gene. *Nature* **380**, 439–442.
7. Kim, J.K., *et al*., & Ferrara, N. (1993). Inhibition of vascular endothelial growth factor-induced angiogenesis suppresses tumour growth *in vivo*. *Nature* **362**, 841–844.
8. Aiello, L.P., *et al*., & King, G. (1994). Vascular endothelial growth in occular fluid of patients with diabetic retinopathy and other retinal disorders. *N. Engl. J. Med.* **331**, 1480–1487.
9. Adamis, A.P., *et al*., & Yeo, K.-T. (1994). Increased vascular endothelial growth factor in the vitreous of eyes with proliferative diabetic retinopathy. *Am. J. Ophthalmol.* **118**, 445–450.
10. Houck, K.A., Ferrara, N., Winer, J., Cachianes, G., Li, B. & Leung, D.W. (1991). The vascular endothelial growth factor family: identification of a fourth molecular species and characterization of alternative splicing of RNA. *Mol. Endocrinol.* **5**, 1806–1814.
11. Tischler, E., *et al*., & Abraham, J.A. (1991). The human gene for vascular endothelial growth factor. Multiple protein forms are encoded through alternative splicing of RNA. *J. Biol. Chem.* **266**, 11947–11954.
12. Keyt, B.A., *et al*., & Ferrara, N. (1996). The carboxyl-terminal domain of vascular endothelial growth factor is critical for its mitogenic potency. *J. Biol. Chem.* **271**, 7788–7795.
13. Leung, D.W., Cachianes, G., Kuang, W.-J., Goeddel, D.V. & Ferrara, N. (1989). Vascular endothelial growth factor is a secreted angiogenic mitogen. *Science* **246**, 1306–1309.
14. Keck, P.J., *et al*., & Connolly, D.T. (1989). Vascular permeability factor, an endothelial cell mitogen related to PDGF. *Science* **246**, 1309–1312.
15. Maglione, D., Guerriero, V., Viglietto, G., Delli-Bovi, P. & Persico, M.G. (1991). Isolation of a human placenta cDNA coding for a protein related to the vascular permeability factor. *Proc. Natl. Acad. Sci. USA* **88**, 9267–9271.
16. Olofsson, B., *et al*., & Eriksson, U. (1996). Vascular endothelial growth factor B, a novel growth factor for endothelial cells. *Proc. Natl. Acad. Sci. USA* **93**, 2576–2581.
17. Joukov, V., *et al*., & Alitalo, K. (1996). A novel vascular endothelial growth factor, VEGF-C, is a ligand for the Flt4 (VEGFR-3) and KDR (VEGFR-2) receptor kinases. *EMBO J.* **15**, 290–298.
18. Lee, J., Gray, A., Yuan, J., Luoh, S.-M., Avraham, H. & Wood, W.I. (1996). Vascular endothelial growth factor-related protein: a ligand and specific activator of the tyrosine kinase receptor Flt-4. *Proc. Natl. Acad. Sci. USA* **93**, 1988–1992.
19. Jeltsch, M., *et al*., & Alitalo, K. (1997). Hyperplasia of lymphatic vessels in VEGF-C transgenic mice. *Science* **276**, 1423–1425.
20. De Vries, C., Escobedo, J.A., Ueno, H., Houck, K., Ferrara, N. & Williams, L.T. (1992). The fms-like tyrosine kinase, a receptor for vascular endothelial growth factor. *Science* **255**, 989–991.
21. Park, J.E., Keller, G.A. & Ferrara, N. (1993). The vascular endothelial growth factor (VEGF) isoforms: differential deposition into the subepithelial extracellular matrix and bioactivity of extracellular matrix-bound VEGF. *Mol. Biol. Cell.* **4**, 1317–1326.
22. Keyt, B.A., *et al*., & Ferrara, N. (1996). Identification of vascular endothelial growth factor determinants for binding KDR and FLT-1 receptors. *J. Biol. Chem.* **271**, 5638–5646.
23. Park, J.E., Chen, H., Winer, J., Houck, K. & Ferrara, N. (1994). Placenta growth factor. Potentiation of vascular endothelial growth factor bioactivity, *in vitro* and *in vivo*, and high affinity binding to Flt-1 but not to Flk-1/KDR. *J. Biol. Chem.* **269**, 25646–25654.
24. Mustonen, T. & Alitalo, K. (1995). Endothelial receptor tyrosine kinases involved in angiogenesis. *J. Cell. Biol.* **129**, 895–898.
25. Muller, Y.A., Li, B., Christinger, H.W., Wells, J.A., Cunningham, B.C. & De Vos, A.M. (1997). Vascular endothelial growth factor: crystal structure and functional mapping of the kinase domain receptor binding site. *Proc. Natl. Acad. Sci. USA* **94**, 7192–7197.
26. Christinger, H.W., *et al*., & De Vos, A.M. (1996). Crystallization of the receptor binding domain of vascular endothelial growth factor. *Proteins* **26**, 353–357.
27. Sun, P.D. & Davies, D.R. (1995). The cystine-knot growth-factor superfamily. *Annu. Rev. Biophys. Biomol. Struct.* **24**, 269–291.
28. McDonald, N.Q. & Hendrickson, W.A. (1993). A structural superfamily of growth factors containing a cystine knot motif. *Cell* **73**, 421–424.
29. Murray-Rust, J., *et al*., & Bradshaw, R.A. (1993). Topological similarities in TGF-β2, PDGF-BB and NGF define a superfamily of polypeptide growth factors. *Structure* **1**, 153–159.
30. Oefner, C., D'Arcy, A., Winkler, F.K., Eggimann, B. & Hosang, M. (1992). Crystal structure of human platelet-derived growth factor BB. *EMBO J.* **11**, 3921–3926.
31. Hinck, A.P., *et al*., & Torchia, D.A. (1996). Transforming growth factor β1: three dimensional structure in solution and comparison with the X-ray structure of transforming growth factor β2. *Biochemistry* **35**, 8517–8534.
32. Daopin, S., Li, M. & Davies, D.R. (1993). Crystal structure of TGF-β2 refined at 1.8 Å resolution. *Proteins* **17**, 176–192.
33. Schlunegger, M.P. & Grütter, M.G. (1993). Refined crystal structure of human transforming growth factor-β2 at 1.95 Å resolution. *J. Mol. Biol.* **231**, 445–458.
34. Mittl, P.R.E., Priestle, J.P., Cox, D.A., McMaster, G., Cerletti, N. & Grütter, M.G. (1996). The crystal structure of TGF-β3 and comparison to TGF-β2: implications for receptor binding. *Protein Sci.* **5**, 1261–1271.
35. Griffith, D.L., Keck, P.C., Sampath, T.K., Rueger, D.C. & Carlson, W.D. (1996). Three-dimensional structure of recombinant human osteogenic protein 1: structural paradigm for the transforming growth factor β superfamily. *Proc. Natl. Acad. Sci. USA* **93**, 878–883.
36. Eigenbrot, C. & Gerber, N. (1997). X-ray structure of glial cell-derived neurotrophic factor at 1.9 Å resolution and implications for receptor binding. *Nat. Struct. Biol.* **4**, 435–438.
37. McDonald, N.Q., Lapatto, R., Murray-Rust, J., Gunning, J., Wlodawer, A. & Blundell, T.L. (1991). New protein fold revealed by a 2.3 Å resolution crystal structure of nerve growth factor. *Nature* **354**, 411–414.
38. Holland, D.R., Cousens, L.S., Meng, W. & Matthews, B.W. (1994). Nerve growth factor in different crystal forms displays structural flexibility and reveals zinc binding sites. *J. Mol. Biol.* **239**, 385–400.
39. Lapthorn, A.J., *et al*., & Isaacs, N.W. (1994). Crystal structure of human chorionic gonadotropin. *Nature* **369**, 455–461.

40. Wu, H., Lustbader, J.W., Liu, Y., Canfield, R.E. & Hendrickson, W.A. (1994). Structure of human chorionic gonadotropin at 2.6 Å resolution from MAD analysis of the selenomethionyl protein. *Structure* **2**, 545–558.
41. Read, R.J. (1986). Improved fourier coefficients for maps using partial structures with errors. *Acta Cryst. A* **42**, 140–149.
42. Laskowski, R.A., MacArthur, M.W., Moss, D.S. & Thornton, J.M. (1993). Procheck: a program to check the stereochemical quality of protein structures. *J. Appl. Cryst.* **26**, 283–291.
43. Isaacs, N.W. (1995). Cystine knots. *Curr. Opin. Struct. Biol.* **5**, 391–395.
44. Muller, Y.A., Schumacher, G., Rudolph, R. & Schulz, G.E. (1994). The refined structures of a stabilized mutant and of wild-type pyruvate oxidase from *Lactobacillus plantarum*. *J. Mol. Biol.* **237**, 315–335.
45. Islam, S.A. & Weaver, D.L. (1990). Molecular interactions in protein crystals: solvent accessible surface and stability. *Proteins* **8**, 1–5.
46. Kossiakoff, A.A., Randal, M., Guenot, J. & Eigenbrot, C. (1992). Variability of conformations at crystal contacts in BPTI represent true low-energy structures: correspondence among lattice packing and molecular dynamic structures. *Proteins* **14**, 65–74.
47. Jones, T.A., Zou, J.-Y., Cowan, S.W. & Kjeldgaard, M. (1991). Improved methods for building protein models in electron density maps and the location of errors in these models. *Acta Cryst. A* **47**, 110–119.
48. Qian, S.W., *et al*., & Roberts, A.B. (1996). Binding affinity of transforming growth factor-beta for its type II receptor is determined by the C-terminal region of the molecule. *J. Biol. Chem.* **271**, 30656–30662.
49. Fairbrother, W.J., Champe, M.A., Christinger, H.W., Keyt, B.A. & Starovasnik, M.A. (1997). ^{1}H, ^{13}C and ^{15}N backbone assignment and secondary structure of the receptor-binding domain of vascular endothelial growth factor. *Protein Sci.* **6**, in press.
50. Hyberts, S., Golberg, M.S., Havel, T.F. & Wagner, G. (1992). The solution structure of eglin C based on measurements of many NOEs and coupling constants and its comparison with X-ray structures. *Protein Sci.* **1**, 736–751.
51. Browner, M.F., Fauman, E.B. & Fletterick, R.J. (1992). Tracking conformational states in allosteric transitions of phosphorylase. *Biochemistry* **31**, 11297–11304.
52. Engstrom, U., Engstrom, A., Ernlund, A., Westermark, B. & Heldin, C.-H. (1992). Identification of a peptide antagonist for platelet-derived growth factor. *J. Biol. Chem.* **267**, 16581–16587.
53. LaRochelle, W.J., Pierce, J.H., May-Siroff, M., Giese, N. & Aaronson, S.A. (1992). Five PDGF-B amino acid substitutions convert PDGF-A to PDGF-B-like transforming molecule. *J. Biol. Chem.* **267**, 17074–17077.
54. Cunningham, B.C. & Wells, J.A. (1991). Rational design of receptor-specific variants of human growth hormone. *Proc. Natl. Acad. Sci. USA* **88**, 3407–3411.
55. De Vos, A.M., Ultsch, M. & Kossiakoff, A.A. (1992). Human growth hormone and extracellular domain of its receptor: structure of the complex. *Science* **225**, 306–312.
56. Somers, W., Ultsch, M., De Vos, A.M. & Kossiakoff, A.A. (1994). The X-ray structure of a growth hormone–prolactin receptor complex. *Nature* **372**, 478–481.
57. Otwinowski, Z. (1993). Oscillation data reduction program. In *Proceedings of the CCP4 Study Weekend: Data Collection and Processing*. (Sawyer, L., Isaacs, N. & Bailey, S., eds). pp. 56–62, SERC Daresbury Laboratory, UK.
58. Brünger, A.T., Kuriyan, J. & Karplus, M. (1987). Crystallographic R factor refinement by molecular dynamics. *Science* **235**, 458–460.
59. Brünger, A.T. (1990). Extension of molecular replacement: a new search strategy based on Patterson correlation refinement. *Acta Cryst. A* **46**, 46–57.
60. Matthews, B.W. (1968). Solvent content of protein crystals. *J. Mol. Biol.* **33**, 491–497.
61. CCP4. (1994). The CCP4 suite: programs for protein crystallography. *Acta Cryst. D* **50**, 760–763.
62. Brünger, A.T. (1992). The free R value: a novel statistical quantity for assessing the accuracy of crystal structures. *Nature* **355**, 472–475.
63. Bhat, T.N. & Cohen, G.H. (1984). OMITMAP: an electron density map suitable for the examination of errors in a macromolecular model. *J. Appl. Cryst.* **17**, 244–248.
64. Murshudov, G.N., Vagin, A.A. & Dodson, E.J. (1997). Refinement of macromolecular structures by the maximum-likelihood method. *Acta Cryst. D* **53**, 240–255.
65. Kraulis, P.J. (1991). MOLSCRIPT: a program to produce both detailed and schematic plots of protein structures. *J. Appl. Cryst.* **24**, 946–950.
66. Merrit, E.A. & Murphy, M.E.P. (1994). Raster3D version 2.0, a program for photorealistic molecular graphics. *Acta Cryst. D* **50**, 869–873.
67. Keck, R.G., Berleau, L., Harris, R. & Keyt, B.A. (1997). Disulfide structure of the heparin binding domain in vascular endothelial growth factor: characterization of posttranslational modifications in VEGF. *Arch. Biochem. Biophys.* **344**, 103–113.